Development of a Probability Distribution Model for SCFs in Uniplanar Tubular KT-Joints of Offshore Structures under IPB Moment Loading

Hamid Ahmadi[1*], Mir Amin Mousavi Nezhad Benam[2]

[1] *Faculty of Civil Engineering, University of Tabriz; h-ahmadi@tabrizu.ac.ir*
[2] *Faculty of Engineering, University of Maragheh; amin.mn90@gmail.com*

ABSTRACT

One of the crucial parameters in the fatigue reliability assessment of an offshore structure's tubular joints is the stress concentration factor (SCF). Depending on the joint geometry and loading type, the SCF exhibits considerable scatter which emphasizes the significance of deriving its governing probability distribution function. In the present paper, results of 144 finite element (FE) stress analyses, verified against experimental measurements, were used to develop a set of probability density functions (PDFs) for the SCFs in uniplanar tubular KT-joints under four types of in-plane bending (IPB) moment load cases. Based on a parametric FE investigation, a sample database was created for the chord-side SCFs of central and outer braces; and density histograms were generated for respective samples. Nine theoretical PDFs were fitted to the developed histograms and the maximum likelihood method was applied to evaluate the parameters of fitted PDFs. The Kolmogorov−Smirnov test was applied to each case to assess the goodness of fit. Finally, the Inverse Gaussian and Gamma models were proposed as the governing probability distribution functions for the central- and outer-brace SCFs, respectively. After substituting the values of estimated parameters, 10 fully defined PDFs were presented for the chord-side SCFs of central and outer braces in uniplanar tubular KT-joints under four types of IPB loading.

1. Introduction

Steel circular hollow sections (CHSs) are widely used in the offshore industry for the fabrication of jacket-type oil/gas production platforms. The welded connection among the main member (chord) and branch members (braces) in the space frame of a jacket structure is called a tubular joint (Fig. 1(a)).

Tubular joints are subjected to cyclic stresses due to the wave loading; and consequently they are susceptible to fatigue damage. Hence, to ensure their safety and integrity, fatigue design is crucial. The stress-life (*S–N*) method, based on the hot-spot stress (HSS), i.e. extrapolated geometric stress at the weld toe, is widely used to estimate the fatigue life of the joints. The HSS can be calculated through the multiplication of nominal stress by the stress concentration factor (SCF).

The SCF is defined as the ratio of the local surface stress, at the brace/chord intersection, to the nominal stress in the brace. The value of SCF depends on the joint geometry, loading type, weld size and type, and the considered position for the SCF determination

around the weld profile. Offshore structures are subjected to multi-axis loading; i.e. combined axial, in-plane bending (IPB) and out-of-plane bending (OPB) loads. The approach recommended by API RP2A [1] to calculate the HSS is to sum the products of the nominal stresses due to each load type and the corresponding SCFs. Under any specific loading condition, the SCF value along the weld toe of a tubular joint is mainly determined by the joint geometry (Fig. 1(b)). A set of dimensionless geometrical parameters including α, α_B, β, γ, τ, and ζ are frequently used to relate the behavior of a tubular joint to its geometrical characteristics more easily. These parameters are defined in Fig. 1(c).

Since limiting assumptions should be made on input parameters, a deterministic fatigue analysis usually results in conservative designs. Some of these parameters exhibit considerable scatter. This fact emphasizes the significance of running a reliability analysis in which the key parameters of the problem can be modeled as random variables. The fundamentals of reliability assessment, if properly

applied, can provide immense insight into the performance and safety of the structural system. Regardless of the method used for the fatigue reliability analysis of steel offshore structures (i.e. either *S–N* or fracture mechanics (FM) approach), the probabilistic and statistical measures of the SCF are among the most important input parameters. The SCF shows considerable scatter highlighting the significance of deriving its governing probability distribution function.

In the present research, initially, available literature on deterministic and probabilistic analysis of SCFs was surveyed (Sec. 2). Afterwards, results from 144 finite element (FE) stress analyses, verified using experimental measurements, were used to derive a probability distribution model for chord-side SCFs in uniplanar tubular KT-joints under four different types of IPB loading (Fig. 1(d)). Based on the parametric FE study, a set of samples was generated for the central- and outer-brace SCFs (Sec. 3) and density histograms were created for respective samples (Sec. 4). Nine theoretical probability density functions (PDFs) were fitted to the developed histograms and the maximum likelihood (ML) method was used to evaluate the parameters of fitted distributions (Sec. 5). In each case, the Kolmogorov−Smirnov test was applied to assess the goodness of fit (Sec. 6). Finally, the best-fitted distributions were detected and after substituting the values of estimated parameters, 10 fully defined PDFs were presented for the weld-toe central- and outer-brace SCFs in uniplanar tubular KT-joints under IPB loading (Sec. 7).

2. Literature review

This section surveys the research works on the deterministic and probabilistic analysis of the SCF as a primary parameter in the fatigue design of tubular joints. For other aspects of the design, such as static strength, hysteretic behaviour, fire resistance, and crack considerations, the reader is referred to Yiyi and Wei [2], Choo [3], Lie *et al.* [4], Gao et al. [5], Liu *et al.* [6], Cui and Shao [7], Shao [8], and Nassiraei *et al.* [9], among others.

2.1. Deterministic studies on SCFs

The following three paragraphs summarize the literature available on unstiffened uniplanar joints, unstiffened multi-planar joints, and stiffened joints, respectively.

For uniplanar joints, the reader is referred for example to Efthymiou and Durkin [10], Efthymiou [11], Hellier *et al.* [12], Smedley and Fisher [13], HSE OTH 354 [14], and Karamanos *et al.* [15] (for the SCF calculation at the saddle and crown positions of simple uniplanar T-, Y-, X-, K-, and KT-joints), Gho

and Gao [16], Gao [17], and Gao *et al.* [18] (for the SCF determination in uniplanar overlapped tubular joints), Morgan and Lee [19, 20], Chang and Dover [21, 22], Shao [23, 24], Shao *et al.* [25], and Lotfollahi-Yaghin and Ahmadi [26] (for the study of the SCF *distribution* along the weld toe of various uniplanar joints), and Pang and Zhao [27] (for the investigation of SCFs in dragline tubular joints).

For multi-planar joints, the reader is referred to Karamanos *et al.* [28] and Chiew *et al.* [29] [for the SCF calculation in XX-joints], Wingerde *et al.* [30] [for the SCF determination in KK-joints], Karamanos *et al.* [31] [for the study of SCFs in DT-joints], and Ahmadi *et al.* [32] [for the investigation of SCFs in three-planar tubular KT-joints], among others.

Ramachandra *et al.* [33] studied the effect of geometrical parameters on the SCFs in ring-stiffened tubular T- and Y-joints. Nwosu *et al.* [34] investigated the stress distribution along the brace/chord intersection of internally ring-stiffened tubular T-joints, under the action of axial, IPB, and OPB loads. Ramachandra *et al.* [35] studied the effect of internal ring stiffeners on the fatigue strength of tubular T- and Y-joints. Hoon *et al.* [36] investigated the SCF distributions along the intersections of a doubler-plate reinforced T-joint subjected to combined loadings. Myers *et al.* [37] studied the effect of three different longitudinal stiffeners on the SCFs in jack-up chords. Woghiren and Brennan [38] established a set of parametric formulas to calculate the SCFs in multi-planar tubular KK-joints stiffened by rack plates. Fatigue design equations for tubular KT-joints reinforced with internal ring stiffeners have been proposed by Ahmadi *et al.* [39] for axial loading and Ahmadi and Zavvar [40] for OPB loading.

2.2. Probabilistic studies on SCFs

In his comprehensive paper on the applications of probabilistic FM to offshore structures, Kirkemo [41] assumed that the SCFs follow a lognormal distribution with the CoV of 0.15 and the mean of 2.75 and 2.50 for axial and IPB loads, respectively.

Pillai and Prasad [42] performed a fatigue reliability analysis in time domain for the inspection strategy of fixed offshore structures. They assumed that the SCF has a lognormal distribution with the mean and CoV of 2.50 and 0.15, respectively. They investigated the sensitivity of the random variables that appear in the fatigue failure limit state equation and found that the SCF is one of the most sensitive variables and it accounts for considerable uncertainty in the probability of failure with respect to fatigue. This calls for greater emphasis in accurately determining the probability distribution of SCFs.
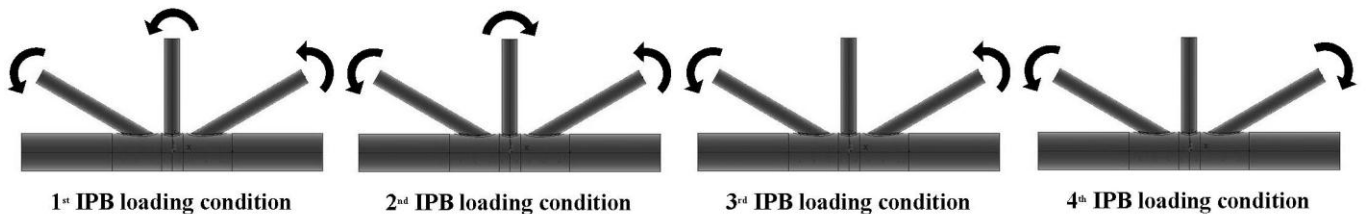
(a) Tubular KT-joints in a jacket structure during the fabrication
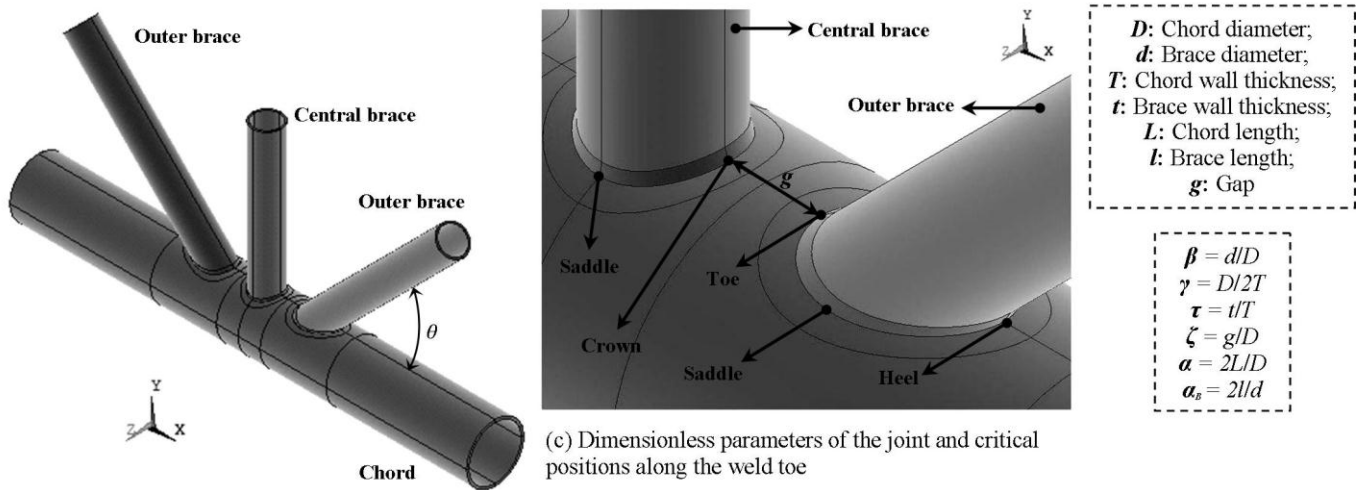
(b) Global geometry

(c) Dimensionless parameters of the joint and critical positions along the weld toe

D: Chord diameter;
d: Brace diameter;
T: Chord wall thickness;
t: Brace wall thickness;
L: Chord length;
l: Brace length;
g: Gap

$\beta = d/D$
$\gamma = D/2T$
$\tau = t/T$
$\zeta = g/D$
$\alpha = 2L/D$
$\alpha_B = 2l/d$

1st **IPB loading condition**   2nd **IPB loading condition**   3rd **IPB loading condition**   4th **IPB loading condition**

(d) Considered in-plane bending (IPB) loading conditions

Fig. 1. Geometrical notation and considered in-plane (IPB) moment load cases for studied uniplanar tubular KT-joints

Mosayyebi and Aghakuchak [43] assumed a normal distribution for the SCFs with the mean of 2.56, 2.50, and 1.90 and the standard deviation of 0.26, 0.25, and 0.19 for axial, IPB, and OPB loads, respectively.

Rajasankar *et al.* [44] applying the reliability analysis to the structural integrity assessment of offshore tubular joints used the lognormal distribution for the SCF with the mean and standard deviation of 10.118 and 2.024, respectively.

Ahmadi and Lotfollahi-Yaghin [45] and Ahmadi *et al.* [46] performed fatigue reliability analyses, based on *S−N* and FM approaches, on two-planar tubular DKT-joints under axial loading. In these papers, a

lognormal distribution was assumed for the SCF with the mean and standard deviation of 2.75 and 0.4125, respectively. Ahmadi and Lotfollahi-Yaghin [47] derived the PDFs for the weld-toe SCFs of the central brace in unstiffened multi-planar tubular DKT-joints under the axial loading. They suggested that the Birnbaum–Saunders distribution is the best probability model for the maximum value of the weld-toe SCF. Ahmadi *et al.* [48, 49] and Ahmadi [50] showed that the Inverse Gaussian, Gamma, and Generalized Extreme Value distributions are the best probability models for the maximum value of the weld-toe SCF in internally ring-stiffened tubular KT-joints subjected to axial, IPB, and OPB loads, respectively. They derived 15 fully defined PDFs for the maximum weld-toe SCFs of central and outer braces, under nine different types of load cases.

3. Development of SCF samples for IPB-loaded uniplanar KT-joints

A total of 36 FE models were generated using ANSYS and analyzed under four types of IPB loads, in order to develop a set of samples for the chord-side SCFs in uniplanar tubular KT-joints subjected to IPB loads. Altogether, 144 FE stress analyses were carried out; and to validate the FE results, experimental measurements were used. Details of FE modeling, parametric investigation, and samples organizing are given in the present section.

3.1. FE modeling and verification
3.1.1. Weld profile geometry

Accurate modeling of the weld profile is one of the most critical factors affecting the accuracy of SCF results. In the present research, the welding size along the brace/chord intersection satisfies the AWS D 1.1 [51] specifications. The dihedral angle (ψ) which is an important parameter in determining the weld thickness is defined as the angle between the chord and brace surface along the intersection curve. The dihedral angle at four typically important positions along the weld toe equals to: $\pi / 2$ (Crown), θ (Heel), $\pi - \cos^{-1}\theta$ (Saddle), and $\pi - \theta$ (Toe); where θ is the outer brace inclination angle (Fig. 1(b)). Details of weld profile modeling according to AWS D 1.1 [51] have been presented by Ahmadi *et al.* [32].

3.1.2. Applied boundary conditions

The fixity condition of chord ends in offshore tubular joints ranges from "almost fixed" to "almost pinned"; and it is generally closer to "almost fixed" [11]. In practice, the value of parameter α in over 60% and 35% of tubular joints is bigger than 20 and 40, respectively [13]. Changing the end restraint from fixed to pinned leads to a maximum increase of 15% in the SCF at the crown position for joints with $\alpha = 6$, and this increment reduces to only 8% for $\alpha = 8$ [20].

In view of the fact that the effect of chord end restraints is only significant for joints with $\alpha < 8$ and high β and γ values, which do not usually found in practice, both chord ends were assumed to be fixed, with the corresponding nodes restrained.

Symmetries and antisymmetries detected in IPB-loaded KT-joints of present study (Fig. 1(d)) are as follows:

- The XY- and YZ-plane geometric symmetries
- The XY-plane loading symmetry under all of four considered IPB loading conditions
- The YZ-plane loading antisymmetry under the 1st, 2nd, and 3rd IPB loading conditions
- The YZ-plane loading symmetry under the 4th IPB loading condition

Hence, in all cases, only one fourth of the entire joint is required to be modeled (Fig. 2(a)). Appropriate symmetric and antisymmetric boundary conditions were defined for the nodes located on the XY- and YZ-planes crossing the centroid of the chord.

3.1.3. Generated mesh

ANSYS element type SOLID95 was used to model the chord, braces, and the weld profiles. These elements have compatible displacements and are well-suited to model curved boundaries. The element is defined by 20 nodes having three degrees of freedom per node and may have any spatial orientation. Using this type of 3-D brick elements, the weld profile can be modeled as a sharp notch. This method will produce more accurate and detailed stress distribution near the intersection in comparison with a simple shell analysis.

To guarantee the mesh quality, a sub-zone mesh generation method was used during the FE modeling. In this method, the entire structure is divided into several different zones according to the computational requirements. The mesh of each zone is generated separately and then the mesh of entire structure is produced by merging the meshes of all the sub-zones. This method can easily control the mesh quantity and quality and avoid badly distorted elements.

As mentioned earlier, to calculate the SCF, the stress at the weld toe should be divided by the nominal stress of the loaded brace. The stresses perpendicular to the weld toe at the extrapolation points are required to be calculated in order to determine the stress at the weld toe position. To extract and extrapolate the stresses perpendicular to the weld toe, as shown in Fig. 2(b), the region between the weld toe and the second extrapolation point was meshed in such a way that each extrapolation point was placed between two nodes located in its immediate vicinity. These nodes are located on the element-generated lines which are perpendicular to the weld toe ($X_\perp$ direction in Fig. 2(d)).

To verify the convergence of FE results, convergence test with different mesh densities was conducted before generating the 36 FE models for the parametric investigation.

3.1.4. Analysis procedure and computation of SCFs

Static analysis of the linearly elastic type is recommended for the SCF determination in tubular joints [52]. The Young's modulus and Poisson's ratio were taken to be 207 GPa and 0.3, respectively.

The weld-toe SCF is defined as:

$$SCF = \sigma_{\perp W} / \sigma_n \tag{1}$$

In Eq. (1), σ_n is the nominal stress of the IPB-loaded brace which is calculated as follows:

$$\sigma_n = \frac{32 d M_{IPB}}{\pi \left[d^4 - (d - 2t)^4 \right]} \tag{2}$$

where M_{IPB} is the in-plane bending moment; and d and t are the brace diameter and wall thickness, respectively.

To determine the SCF, the HSS should be calculated. The HSS is the stress at the weld toe position obtained through the extrapolation of the stresses from the outside of the region influenced by the local weld toe geometry. The location from which the stresses must be extrapolated, *extrapolation region*, depends on the dimensions of the joint and on the position along the intersection. According to the linear extrapolation method recommended by IIW-XV-E [53], the first extrapolation point have to be at a distance of $0.4T$ from the weld toe, and the second point should lie at $1.0T$ further from the first point (Fig. 2(c)).

In Eq. (1), $\sigma_{\perp W}$ is the extrapolated stress at the weld toe position which is perpendicular to the weld toe and is calculated by the following equation:

$$\sigma_{\perp W} = 1.4 \sigma_{\perp E1} - 0.4 \sigma_{\perp E2} \tag{3}$$

where $\sigma_{\perp E1}$ and $\sigma_{\perp E2}$ are the stresses at the first and second extrapolation points along the direction perpendicular to the weld toe, respectively (Fig. 2(c)).

The stress at an extrapolation point is obtained as follows:

$$\sigma_{\perp E} = \frac{\sigma_{\perp N1} - \sigma_{\perp N2}}{\delta_1 - \delta_2} (\Delta - \delta_2) + \sigma_{\perp N2} \tag{4}$$

where $\sigma_{\perp Ni}$ ($i = 1$ and 2) is the nodal stress at the immediate vicinity of the extrapolation point along the direction perpendicular to the weld toe (Eq. (5)); δ_i ($i = 1$ and 2) is the distance between the weld toe and the considered node inside the extrapolation region (Eq. (6)); and Δ equals to $0.4T$ and $1.4T$ for the first and second extrapolation points, respectively (Fig. 2(d)).

$$\sigma_{\perp N} = \sigma_x l_1^2 + \sigma_y m_1^2 + \sigma_z n_1^2 + 2 \left(\tau_{xy} l_1 m_1 + \tau_{yz} m_1 n_1 + \tau_{zx} n_1 l_1 \right) \tag{5}$$

where σ_a and τ_{ab} ($a, b = x, y, z$) are components of the stress tensor which can be extracted from ANSYS analysis results; and l_1, m_1, and n_1 are transformation components.

$$\delta = \sqrt{(x_w - x_n)^2 + (y_w - y_n)^2 + (z_w - z_n)^2} \tag{6}$$

In Eq. (6), (x_n, y_n, z_n) and (x_w, y_w, z_w) are the global coordinates of the considered node inside the extrapolation region and its corresponding node at the weld toe position, respectively.

At the crown, toe, and heel positions, Eq. (5) is simplified as:

$$\sigma_{\perp N} = \sigma_x \tag{7}$$

In the present research, the saddle position was not studied. The reason is that under the IPB loadings, the nominal stress at this position is zero and hence the determination of SCFs is not needed.

In order to facilitate the SCF calculation, above formulation was implemented in a *macro* developed by the ANSYS Parametric Design Language (APDL). The input data required to be provided by the user of the macro are the node number at the weld toe, the chord thickness, and the numbers of the nodes inside the extrapolation region. These nodes can be introduced using the Graphic user interface (GUI).

3.1.5. Verification of FE results based on experimental data

In order to verify the developed FE modeling procedure, a validating FE model was generated and its outputs were compared with the results of experimental tests conducted by Ahmadi *et al.* [54]. Details of test setup and program are not presented here for the sake of brevity.

The specimen fabricated by Ahmadi *et al.* [54] was tested under the axial loading. In order to verify the FE models using the data extracted from this experiment, the FE model of tested specimen was generated and analyzed under axial loading. The method of geometrical modeling (introducing the chord, braces, and weld profiles), the mesh generation procedure (including the selection of the element type and size), the analysis method, and the method of SCF computation are the same for the validating model and the IPB-loaded joints used here for the parametric study. Hence, the verification of SCFs derived from axially-loaded FE model with corresponding experimental values lends some support to the validity of SCFs derived from IPB-loaded FE models.
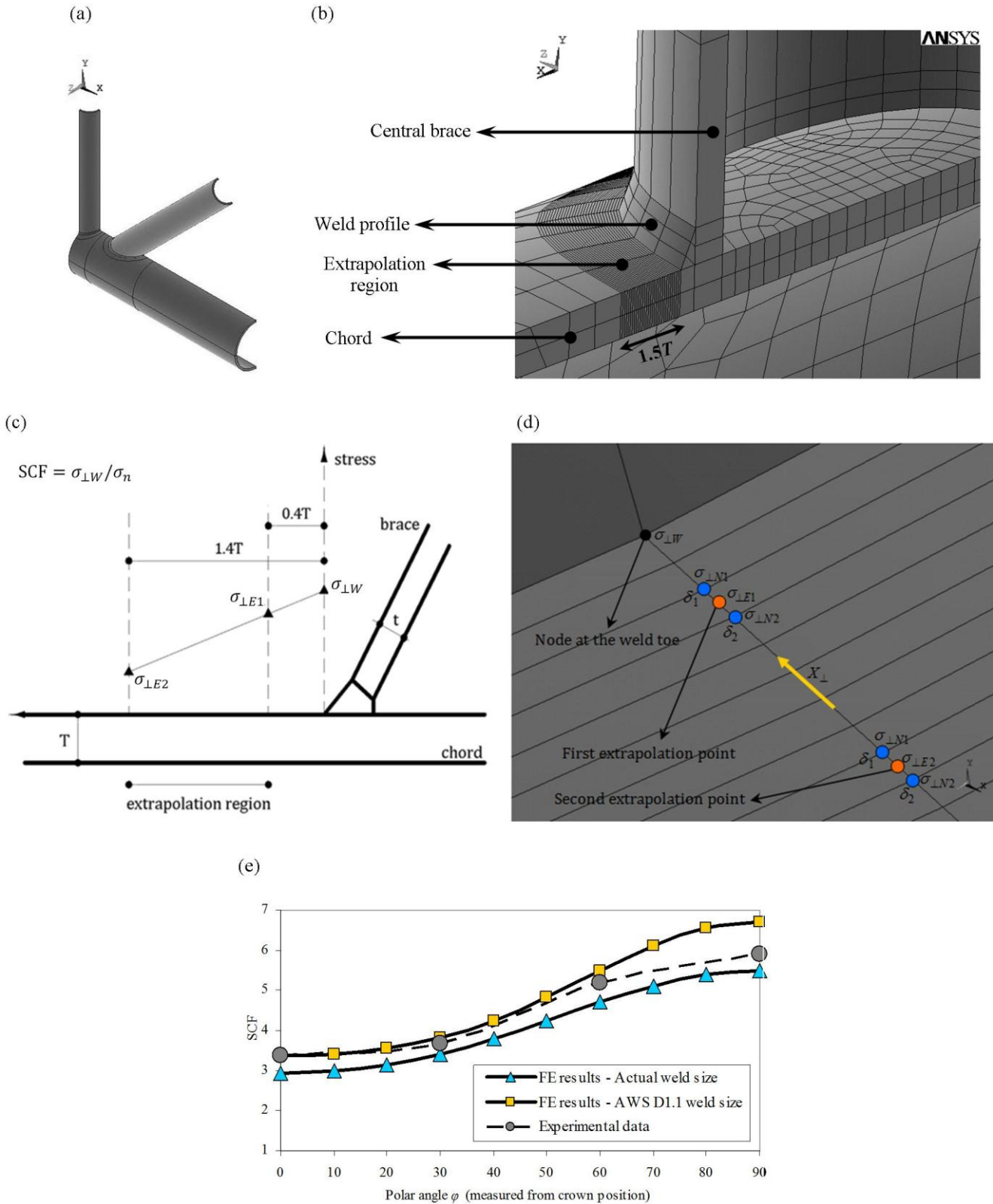
Fig. 2. (a) One fourth of the entire joint required to be modeled, (b) Mesh generated in the regions adjacent to the intersection, (c) Adapted linear extrapolation method, (d) Interpolations and extrapolations necessary to determine SCFs based on the stresses perpendicular to the weld toe, (e) Distribution of chord-side SCFs along the central brace/chord intersection of a uniplanar KT-joint: Comparison of the experimental measurements with the FE results

Moreover, in order to make sure that the IPB moment loading was correctly defined in ANSYS, nominal stresses obtained from the software were verified against the results of theoretical solid mechanics relations.

In Fig. 2(e), experimental data and FE results have been compared. In this figure, the SCF distribution along the central brace/chord intersection is presented. The polar angle (φ) along the 360˚ curve of the weld path is measured from the crown position. Hence,

values of φ at the crown and saddle positions are 0° and 90°, respectively. Due to the symmetry, only one fourth of the entire 360° SCF distribution is depicted.

The FE analysis predicts a stiffer structure than the actual one. This is expected, as the finite element model forces the structure into specific modes of displacement and effectively yields a stiffer model than the actual structure. This additional stiffness of the chord member yields to smaller deformation and consequently to lower SCFs of the chord member, compared to the experimental results. However, this does not mean that the results of FE models used for the parametric study are under-predicting. The reason is that weld sizes in FE models used for the parametric study satisfy the AWS D 1.1 [51] specifications and thus are smaller than weld sizes typically found in yard practice. Hence, as depicted in Fig. 2(e), the SCFs obtained from these models are higher than SCFs actually occurring in practice; and the FE results are even somewhat conservative.

As can be seen in Fig. 2(e), there is a good agreement between the test results and FE predictions. Hence, generated FE models can be considered to be accurate enough to provide valid results.

3.2. Details of parametric study

In order to prepare a sample database for the SCFs in uniplanar KT-joints subjected to four types of IPB loading (Fig. 1(d)), 36 models were generated and analyzed using ANSYS. The aim was to investigate the effects of dimensionless geometrical parameters on the chord-side SCFs at the crown, toe, and heel positions. As mentioned earlier, the saddle position was not studied. The reason is that under the IPB loading, the nominal stress at this position is zero and hence the determination of SCFs is not required.

Different values assigned to the parameters β, γ, τ, and θ are as follows: $\beta = 0.4, 0.6$; $\gamma = 12, 24$; $\tau = 0.4$,

0.7, 1.0; and $\theta = 30°, 45°, 60°$. These values cover the practical ranges of dimensionless parameters typically found in tubular joints of offshore jacket structures. Providing that the gap between the central and outer braces is not very large, the relative gap ($\zeta = g / D$) has no considerable effect on the SCF values in a tubular KT-joint. The validity range for this conclusion is $0.2 \leq \zeta \leq 0.6$ [26]. Hence, a typical value of $\zeta = 0.3$ was designated for all joints. Sufficiently long chord greater than six chord diameters (i.e. $\alpha \geq 12$) should be used to ensure that the stresses at the brace/chord intersection are not affected by the chord's boundary conditions [11]. Hence, in this study, a realistic value of $\alpha = 16$ was designated for all the models. The brace length has no effect on SCFs when the parameter α_B is greater than a critical value [21]. According to Chang and Dover [55], this critical value is about 6. In the present study, in order to avoid the effect of short brace length, a realistic value of $\alpha_B = 8$ was assigned for all joints.

3.3. Organizing the SCF sample database

The SCFs extracted from the results of 144 FE stress analyses were organized as 10 samples for further statistical and probabilistic analyses. Samples 1−3 included the weld-toe SCFs under the 1st IPB loading condition at the crown position of the central (vertical) brace, heel position of the outer (inclined) brace, and toe position of the outer brace, respectively. Samples 4−6 included the SCFs at the same positions under the 2nd IPB loading condition. Samples 7 and 8 included the weld-toe SCFs under the 3rd IPB loading condition at the heel and toe positions of the outer brace, respectively; and finally Samples 9 and 10 included the SCFs at the same positions under the 4th IPB loading condition.

Table 1. Statistical measures of the generated samples

Statistical measure	SCF samples									
	Sample 1	Sample 2	Sample 3	Sample 4	Sample 5	Sample 6	Sample 7	Sample 8	Sample 9	Sample 10
	1st loading condition; central-brace crown SCFs	1st loading condition; outer-brace heel SCFs	1st loading condition; outer-brace toe SCFs	2nd loading condition; central-brace crown SCFs	2nd loading condition; outer-brace heel SCFs	2nd loading condition; outer-brace toe SCFs	3rd loading condition; outer-brace heel SCFs	3rd loading condition; outer-brace toe SCFs	4th loading condition; outer-brace heel SCFs	4th loading condition; outer-brace toe SCFs
n	36	36	36	36	36	36	36	36	36	36
μ	3.1583	2.483575	2.006375	3.2058	2.350050	2.174261	2.402727	2.084419	2.349544	2.217644
σ	1.2866	1.110180	1.226375	1.2648	1.177201	1.040296	1.129699	1.110468	1.118688	1.133185
α_3	0.5911	0.380664	0.865928	0.5643	0.534715	0.741863	0.499764	0.902267	0.460881	0.877139
α_4	2.2601	2.337246	3.043278	2.1843	2.536123	2.942387	2.518453	3.190353	2.524777	3.101219

Values of the size (n), mean (μ), standard deviation (σ), coefficient of skewness (α_3), and coefficient of kurtosis (α_4) for these samples are listed in Table 1. The value of μ shows that the central-brace SCFs are generally higher than the corresponding outer-brace SCFs. The value of α_3 for all samples is positive which means that the probability distribution for all samples is expected to have a longer tail on the right, which is toward increasing values, than on the left. Moreover, in Samples 3, 8, and 10, the value of α_4 is greater than three meaning that the probability distribution is expected to be sharp-peak (leptokurtic) for these three samples which are all related to the SCFs at the toe position. In other SCF samples, the value of α_4 is smaller than three implying that the probability distribution is expected to be mild-peak (platykurtic) for these seven samples.

4. Generating the density histograms based on Freedman−Diaconis rule

To generate a density histogram, the range (R) is divided into a number of classes and the number of occurrences in each class is counted and tabulated. These are called frequencies. Then, the relative frequency of each class can be obtained through dividing its frequency by the sample size. Afterwards, the density is calculated for each class through dividing the relative frequency by the class width. The width of classes is usually made equal to facilitate interpretation.

Care should be exercised in the choice of the number of classes (n_c). Too few will cause an omission of some important features of the data; too many will not give a clear overall picture because there may be high frequency fluctuations. One of the widely accepted rules to determine the number of classes is Freedman−Diaconis rule expressed as [56]:

$$n_c = \frac{R\left(n^{1/3}\right)}{2\left(\text{IQR}\right)} \tag{8}$$

where R is the range of sample data, n is the sample size, and IQR is the interquartile range calculated as:

$$\text{IQR} = Q_3 - Q_1 \tag{9}$$

where Q_1 is the lower quartile which is the median of lower half of the data; and likewise, Q_3 is the upper quartile that is the median of upper half of the data.

5. PDF fitting using the maximum likelihood method

Nine different PDFs were fitted to the density histograms to assess the degree of fitting of various distributions to the SCF samples. Fig. 3 is presented as an example showing the fits for the 1st loading condition. In each case, distribution parameters were estimated using the maximum likelihood (ML) method. Results are given in Table 2. The ML

procedure is an alternative to the method of moments. As a means of finding an estimator, statisticians often give it preference. For a random variable X with a known PDF, $f_X(x)$, and observed values $x_1, x_2, \ldots, x_n$, in a random sample of size n, the likelihood function of ω, where ω represents the vector of unknown parameters, is defined as:

$$L(\omega) = \prod_{i=1}^{n} f_X\left(x_i \mid \omega\right) \tag{10}$$

The objective is to maximize $L(\omega)$ for the given data set. It is done by taking m partial derivatives of $L(\omega)$, where m is the number of parameters, and equating them to zero. Then the maximum likelihood estimators (MLEs) of the parameter set ω can be found from the solutions of equations. In this way the greatest probability is given to the observed set of events, provided that the true form of the probability distribution is known.

6. Assessing of the goodness-of-fit based on the Kolmogorov−Smirnov test

The Kolmogorov−Smirnov goodness-of-fit test is a nonparametric test that relates to the cumulative distribution function (CDF) of a continuous variable. The test statistic, in a two-sided test, is the maximum absolute difference (which is usually the vertical distance) between the empirical and hypothetical CDFs. For a continuous variate X, let $x_{(1)}, x_{(2)}, \ldots, x_{(n)}$ represent the order statistics of a sample of the size n, that is, the values arranged in increasing order. The empirical or sample distribution function $F_n(x)$ is a step function. This gives the proportion of values not exceeding x and is defined as:

$$
\begin{aligned}
F_n(x) &= 0, \\
&\quad \text{For } x < x_{(1)} \\
&= k/n, \\
&\quad \text{For } x_{(k)} \le x < x_{(k+1)} \qquad k = 1, 2, \ldots, n-1 \\
&= 1, \\
&\quad \text{For } x \ge x_{(n)}
\end{aligned} \tag{11}
$$

Let $F_0(x)$ denote a completely specified theoretical continuous CDF. The null hypothesis H_0 is that the true CDF of X is the same as $F_0(x)$. That is, under the null hypothesis:

$$\lim_{n \to \infty} \Pr\left[F_n(x) = F_0(x)\right] = 1 \tag{12}$$

The test criterion is the maximum absolute difference between $F_n(x)$ and $F_0(x)$, formally defined as:

$$d_n = \sup_x \left| F_n(x) - F_0(x) \right| \tag{13}$$

Theoretical continuous CDFs fitted to the empirical distribution functions of generated samples have been shown in Fig. 4 for the 1st loading condition. The fits of the other loading conditions are not presented here for the sake of brevity.
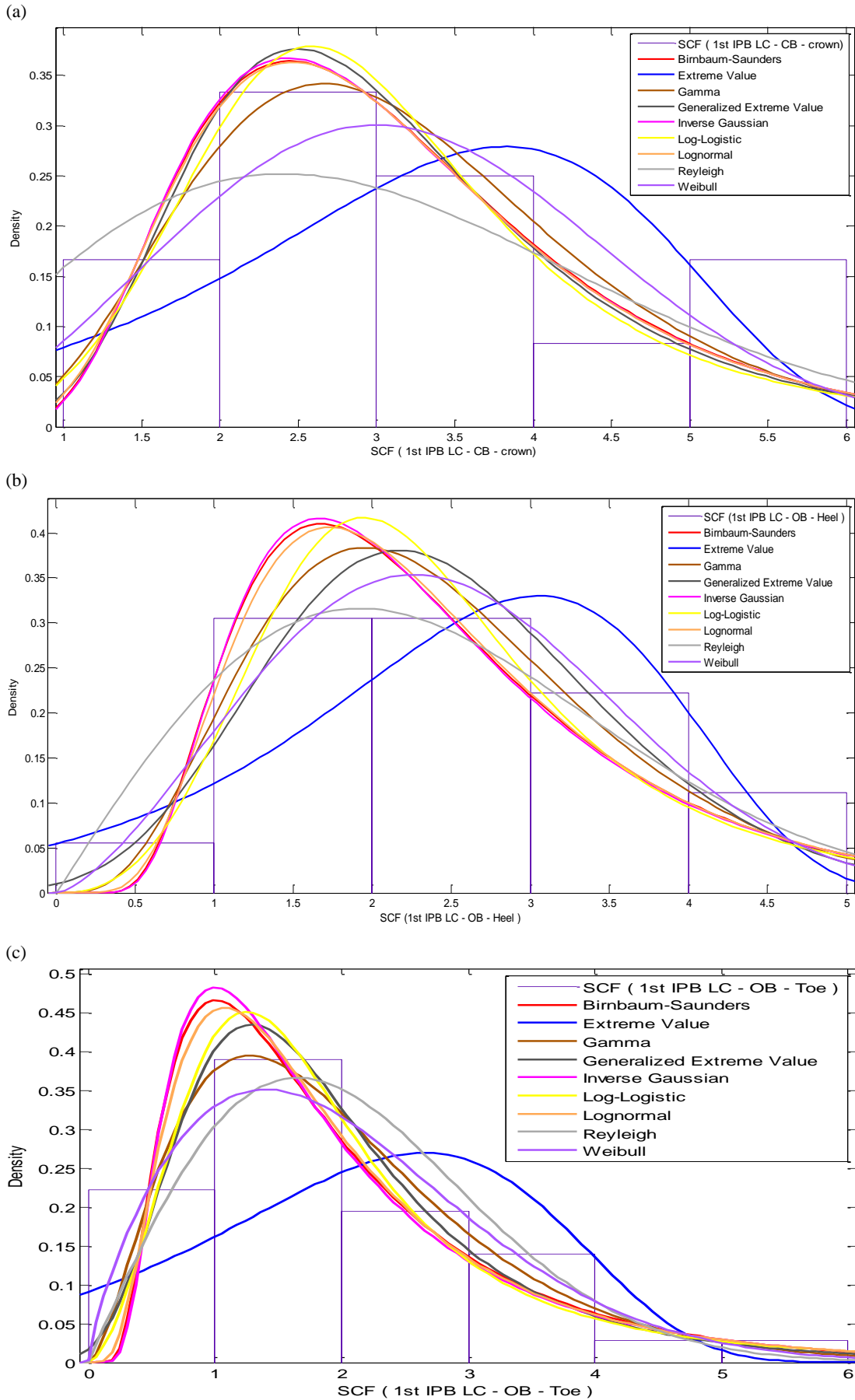
(a)

(b)

(c)

Fig. 3. Probability density functions fitted to the generated histograms: (a) Sample 1 (1ˢᵗ *ILC*, *CB*, *C*), (b) Sample 2 (1ˢᵗ *ILC*, *OB*, *H*), (c) Sample 3 (1ˢᵗ *ILC*, *OB*, *T*); [KEY: *ILC*: IPB loading condition; *CB*: Central brace; *OB*: Outer brace; *C*: Crown; *H*: Heel; *T*: Toe]
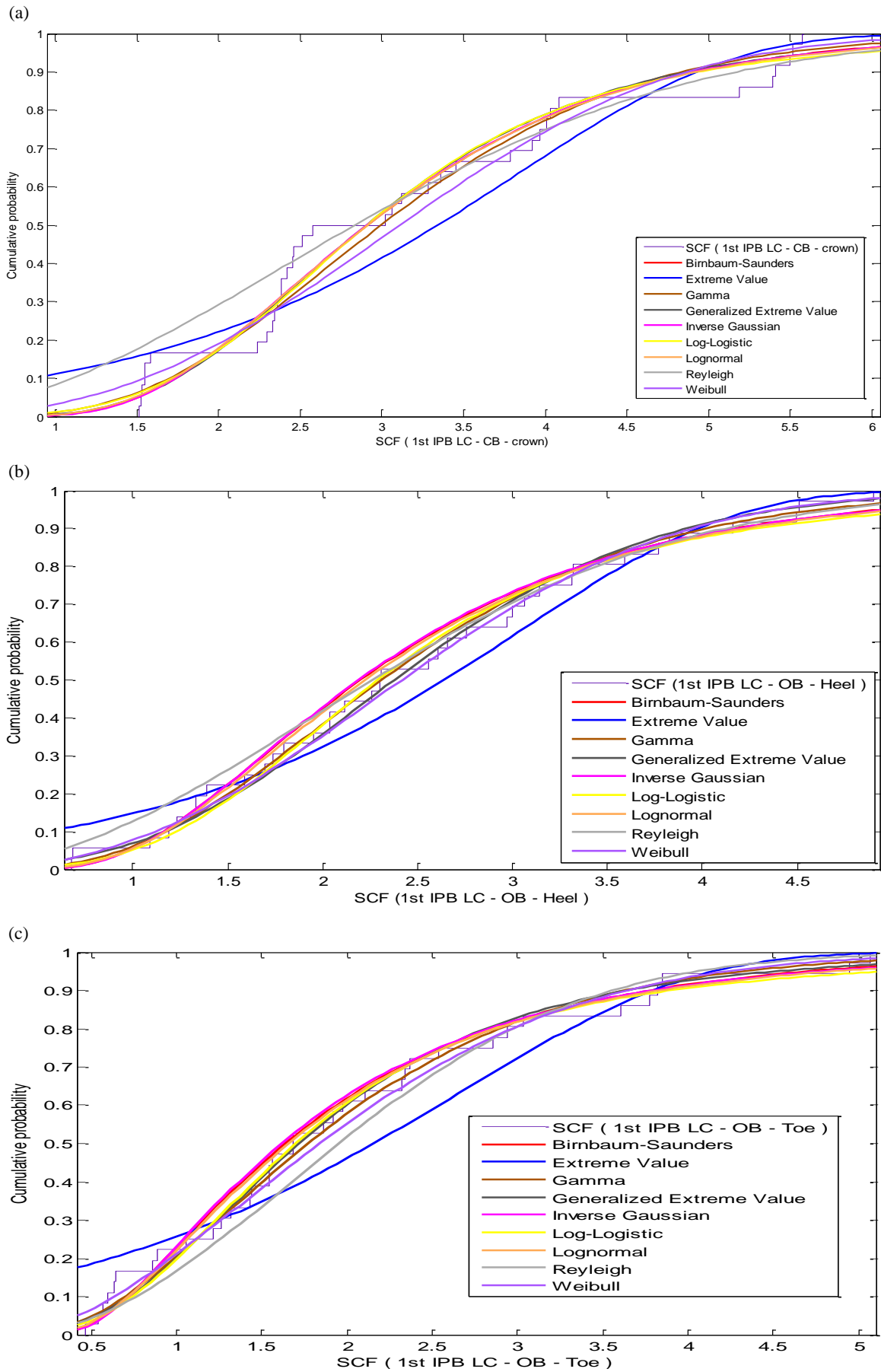
(a)

(b)

(c)

Fig. 4. Theoretical continuous CDFs fitted to the empirical CDFs of generated samples: (a) Sample 1 (1st *ILC*, *CB*, *C*), (b) Sample 2 (1st *ILC*, *OB*, *H*), (c) Sample 3 (1st *ILC*, *OB*, *T*); [KEY: *ILC*: IPB loading condition; *CB*: Central brace; *OB*: Outer brace; *C*: Crown; *H*: Heel; *T*: Toe]

Table 2. Estimated parameters for PDFs fitted to the density histograms of SCF samples

Fitted PDF	Parameters	Estimated values									
		Sample 1	Sample 2	Sample 3	Sample 4	Sample 5	Sample 6	Sample 7	Sample 8	Sample 9	Sample 10
		1st loading condition; central-brace crown SCFs	1st loading condition; outer-brace heel SCFs	1st loading condition; outer-brace toe SCFs	2nd loading condition; central-brace crown SCFs	2nd loading condition; outer-brace heel SCFs	2nd loading condition; outer-brace toe SCFs	3rd loading condition; outer-brace heel SCFs	3rd loading condition; outer-brace toe SCFs	4th loading condition; outer-brace heel SCFs	4th loading condition; outer-brace toe SCFs
Birnbaum-Saunders	β_0	2.91356	2.19859	1.63586	2.97356	2.01255	1.92637	2.1013	1.80848	2.03462	1.95107
	γ_0	0.409872	0.507157	0.670526	0.395299	0.575938	0.5063	0.533229	0.551696	0.553259	0.522361
Extreme Value	μ	3.82526	3.04891	2.65581	3.85988	2.95737	2.72021	2.98403	2.67433	2.92326	2.81839
	σ	1.31817	1.11427	1.36567	1.28543	1.22555	1.13623	1.16728	1.24871	1.15178	1.26591
Gamma	a	6.36486	4.69865	2.74885	6.7897	3.77883	4.50136	4.30773	3.77739	4.1021	4.13153
	b	0.496209	0.528572	0.729895	0.472163	0.621899	0.483023	0.557771	0.551815	0.572767	0.536761
Generalized Extreme Value	k	0.0485228	-0.139079	0.133884	0.0556917	-0.061384	0.00912559	-0.0885775	0.102537	-0.109344	0.103034
	σ	0.978184	0.976381	0.853723	0.959277	0.974958	0.806612	0.955875	0.787767	0.96315	0.805316
	μ	2.54056	2.02909	1.39382	2.59335	1.83388	1.69681	1.9194	1.5444	1.87949	1.66516
Inverse Gaussian	μ	3.1583	2.48358	2.00637	3.20584	2.35005	2.17426	2.40273	2.08442	2.34954	2.21764
	λ	1.28664	9.07255	4.01164	19.7446	6.54231	7.97114	7.88962	6.36409	7.1303	7.60838
Log-logistic	μ	1.06775	0.829664	0.528206	1.08616	0.748525	0.676671	0.785843	0.606876	0.763577	0.676465
	σ	0.24037	0.283776	0.378692	0.233558	0.318281	0.284741	0.294587	0.312846	0.303487	0.29805
Lognormal	μ	1.06943	0.799528	0.503545	1.08953	0.716324	0.661518	0.756067	0.596323	0.727409	0.670571
	σ	0.40992	0.499979	0.654463	0.395875	0.562831	0.500189	0.52352	0.543769	0.54136	0.51643
Rayleigh	b	2.40669	1.91917	1.65647	2.43236	1.85338	1.69994	1.87268	1.66489	1.83536	1.7559
Weibull	a	3.56427	2.80749	2.26454	3.61317	2.66087	2.46314	2.71887	2.36415	2.6581	2.51581
	b	2.68928	2.44854	1.75868	2.78139	2.15894	2.26758	2.31158	2.03656	2.27826	2.12555

A large value of this statistic (d_n) indicates a poor fit. Hence, acceptable values should be known. The critical values $D_{n,\xi}$ for large samples, say $n > 35$, are $(1.3581 / \sqrt{n})$ and $(1.6276 / \sqrt{n})$ for $\xi = 0.05$ and 0.01, respectively [56] where ξ is the significance level.

Results of the Kolmogorov−Smirnov test for the 10 prepared samples were tabulated. As an example, results of the test for Sample 1 are given in Table 3. Outputs for the other samples are not presented here for the sake of brevity. Results of the Kolmogorov−Smirnov test indicated that the Generalized Extreme Value distribution has the smallest value of the test statistic (d_n) for Samples 4, 7, and 9; while the Weibull distribution has the smallest d_n value for Samples 2 and 3; and the Gamma distribution has the smallest d_n for Samples 5 and 10. It was also observed that the Inverse Gaussian, Log-logistic, and Birnbaum−Saunders distributions have the smallest d_n for Samples 1, 6, and 8, respectively. Hence, they are the best-fitted distributions for the corresponding SCF samples (Fig. 5).

Table 3. Results of the Kolmogorov-Smirnov goodness-of-fit test for SCF sample 1 (1st loading condition; central-brace crown SCFs)

Fitted distribution	Test statistic	Critical value		Test result	
		$\xi = 0.05$	$\xi = 0.01$	$\xi = 0.05$	$\xi = 0.01$
Birnbaum-Saunders	0.117027			Accept	Accept
Extreme Value	0.178047			Accept	Accept
Gamma	0.140479			Accept	Accept
Generalized Extreme Value	0.117643			Accept	Accept
Inverse Gaussian	0.115216	0.22635	0.27126	Accept	Accept
Log-logistic	0.122583			Accept	Accept
Lognormal	0.116989			Accept	Accept
Rayleigh	0.184410			Accept	Accept
Weibull	0.157745			Accept	Accept
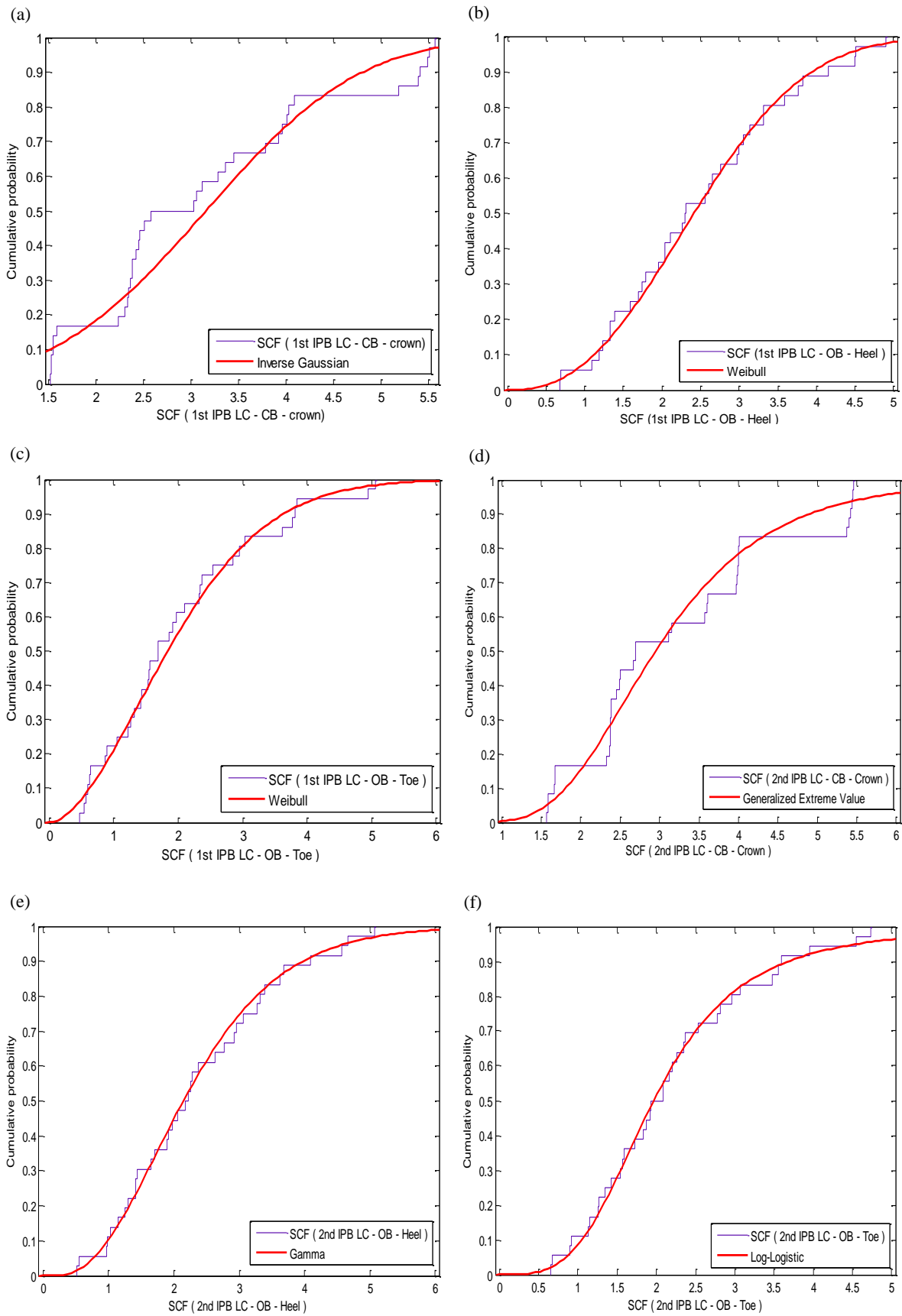
Fig. 5. The best-fitted distributions according to the Kolmogorov−Smirnov test: (a) Sample 1 (1st *ILC*, *CB*, *C*), (b) Sample 2 (1st *ILC*, *OB*, *H*), (c) Sample 3 (1st *ILC*, *OB*, *T*), (d) Sample 4 (2nd *ILC*, *CB*, *C*), (e) Sample 5 (2nd *ILC*, *OB*, *H*), (f) Sample 6 (2nd *ILC*, *OB*, *T*), (g) Sample 7 (3rd *ILC*, *OB*, *H*), (h) Sample 8 (3rd *ILC*, *OB*, *T*), (i) Sample 9 (4th *ILC*, *OB*, *H*), (j) Sample 10 (4th *ILC*, *OB*, *T*); [KEY: *ILC*: IPB loading condition; *CB*: Central brace; *OB*: Outer brace; *C*: Crown; *H*: Heel; *T*: Toe]
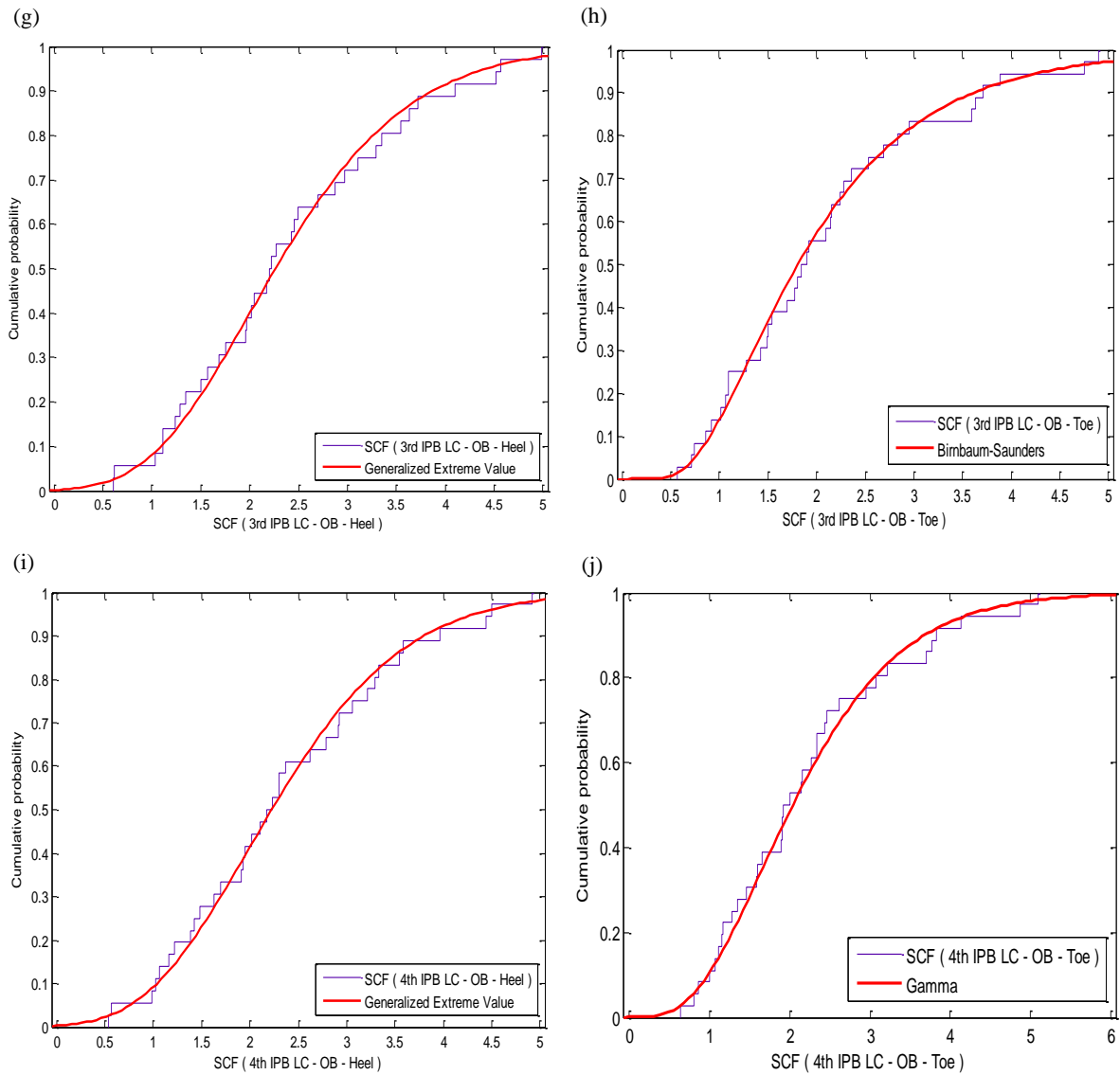
(g)

(h)

(i)

(j)

Fig. 5. *(Continued)*

7. Probability distribution models proposed for the SCFs in IPB-loaded KT-joints

The best fitted distributions for the generated SCF samples were introduced in Sec. 6. It can be seen that the best fitted distributions for these 10 samples include six different models: Generalized Extreme Value, Weibull, Gamma, Inverse Gaussian, Log-logistic, and Birnbaum−Saunders distributions. The diversity of the best-fitted probability models derived for the studied SCFs may practically result in the confusion and difficulty of their application for the fatigue analysis and design. Hence, reducing the number of distribution types proposed for the SCFs might be a good idea. In order to do so, the top three distribution functions for each SCF sample were identified (Table 4). The aim was to propose only two probability models to cover all the central- and outer-brace SCFs. It should be noted that, for each sample, all of the three mentioned functions have acceptable fit according to the Kolmogorov−Smirnov test. After surveying the data presented in Table 4, the Inverse

Gaussian and Gamma models are proposed as the governing probability distribution functions for the central- and outer-brace SCFs, respectively. The difference between the test statistic of the proposed distributions and the best-fitted ones for each sample are presented in Table 5. Using the information presented in Table 5, the analyst is able to make a choice, based on the engineering judgment, between the best-fitted and the proposed probability models for each of the 10 studied cases.

The PDF of the Inverse Gaussian and Gamma distributions are expressed as:

$$f_X(x) = \sqrt{\frac{\lambda}{2\pi x^3}} \exp\left\{-\frac{\lambda}{2\mu^2 x}(x-\mu)^2\right\} \text{(Inv. Gauss.)} \quad (14)$$

$$f_X(x) = \frac{1}{b^a \Gamma(a)} x^{a-1} e^{-x/b} \quad \text{(Gamma)} \quad (15)$$

where $\Gamma(a)$ is the Gamma function defined as:

$$\Gamma(a) = \int_0^\infty e^{-r} r^{a-1} dr \quad (16)$$

Table 4. Best-fitted distributions for the SCF samples based on the results of the Kolmogorov-Smirnov test

	SCF samples									
	Sample 1	Sample 2	Sample 3	Sample 4	Sample 5	Sample 6	Sample 7	Sample 8	Sample 9	Sample 10
Best-fitted distributions	1st loading condition; central-brace crown SCFs	1st loading condition; outer-brace heel SCFs	1st loading condition; outer-brace toe SCFs	2nd loading condition; central-brace crown SCFs	2nd loading condition; outer-brace heel SCFs	2nd loading condition; outer-brace toe SCFs	3rd loading condition; outer-brace heel SCFs	3rd loading condition; outer-brace toe SCFs	4th loading condition; outer-brace heel SCFs	4th loading condition; outer-brace toe SCFs
#1	Inverse Gaussian	Weibull	Weibull	Generalized Extreme Value	Gamma	Log-logistic	Generalized Extreme Value	Birnbaum-Saunders	Generalized Extreme Value	Gamma
#2	Lognormal	Generalized Extreme Value	Gamma	Inverse Gaussian	Weibull	Generalized Extreme Value	Gamma	Inverse Gaussian	Log-logistic	Log-logistic
#3	Birnbaum-Saunders	Gamma	Generalized Extreme Value	Lognormal	Rayleigh	Gamma	Log-logistic	Lognormal	Gamma	Generalized Extreme Value

Table 5. Comparison of the test statistics for the proposed and the best-fitted distributions based on the results of the Kolmogorov-Smirnov test

Test statistic	SCF samples									
	Sample 1	Sample 2	Sample 3	Sample 4	Sample 5	Sample 6	Sample 7	Sample 8	Sample 9	Sample 10
Best-fitted distribution	0.115216 (Inverse Gaussian)	0.065779 (Weibull)	0.079255 (Weibull)	0.119851 (Generalized Extreme Value)	0.063538 (Gamma)	0.051124 (Log-logistic)	0.057193 (Generalized Extreme Value)	0.072604 (Birnbaum-Saunders)	0.060320 (Generalized Extreme Value)	0.075240 (Gamma)
Proposed distribution	0.115216 (Inverse Gaussian)	0.070696 (Gamma)	0.082681 (Gamma)	0.123130 (Inverse Gaussian)	0.063538 (Gamma)	0.060784 (Gamma)	0.071462 (Gamma)	0.080282 (Gamma)	0.071798 (Gamma)	0.075240 (Gamma)
Difference	0%	7.5%	4.3%	2.7%	0%	19%	25%	10.5%	19%	0%

After substituting the values of estimated parameters from Table 2, following probability density functions are proposed for the weld-toe SCFs of the central and outer braces in uniplanar tubular KT-joints subjected to the four considered IPB load cases defined in Fig. 1(d):

- **Weld-toe SCFs of the central brace:**

1st IPB loading condition − Crown position:

$$f_X(x) = \sqrt{\frac{0.64332}{\pi x^3}} \exp\left\{-\frac{0.064494145}{x}(x-3.1583)^2\right\} \tag{17}$$

2nd IPB loading condition − Crown position:

$$f_X(x) = \sqrt{\frac{9.8723}{\pi x^3}} \exp\left\{-\frac{0.960582472}{x}(x-3.20584)^2\right\} \tag{18}$$

- **Weld-toe SCFs of the outer brace:**

1st IPB loading condition − Heel position:

$$f_X(x) = 1.298594855 x^{3.69865} e^{-x/0.528572} \tag{19}$$

1st IPB loading condition − Toe position:

$$f_X(x) = 1.478776153 x^{1.74885} e^{-x/0.729895} \tag{20}$$

2nd IPB loading condition − Heel position:

$$f_X(x) = 1.314984484 x^{2.77883} e^{-x/0.621899} \tag{21}$$

2nd IPB loading condition − Toe position:

$$f_X(x) = 2.270439733 x^{3.50136} e^{-x/0.483023} \tag{22}$$

3rd IPB loading condition − Heel position:

$$f_X(x) = 1.381972165 x^{3.30773} e^{-x/0.557771} \tag{23}$$

3rd IPB loading condition − Toe position:

$$f_X(x) = 2.067828757 x^{2.77739} e^{-x/0.551815} \tag{24}$$

4th IPB loading condition − Heel position:

$$f_X(x) = 1.439835091 x^{3.1021} e^{-x/0.572767} \tag{25}$$

4th IPB loading condition − Toe position:

$$f_X(x) = 1.842725568 x^{3.13153} e^{-x/0.536761} \tag{26}$$

where X denotes the SCF as a random variable and x represents its values.

Developed PDFs, shown in Fig. 6, can be adapted in the fatigue reliability analysis of uniplanar tubular KT-joints under the IPB loading commonly found in offshore jacket structures.
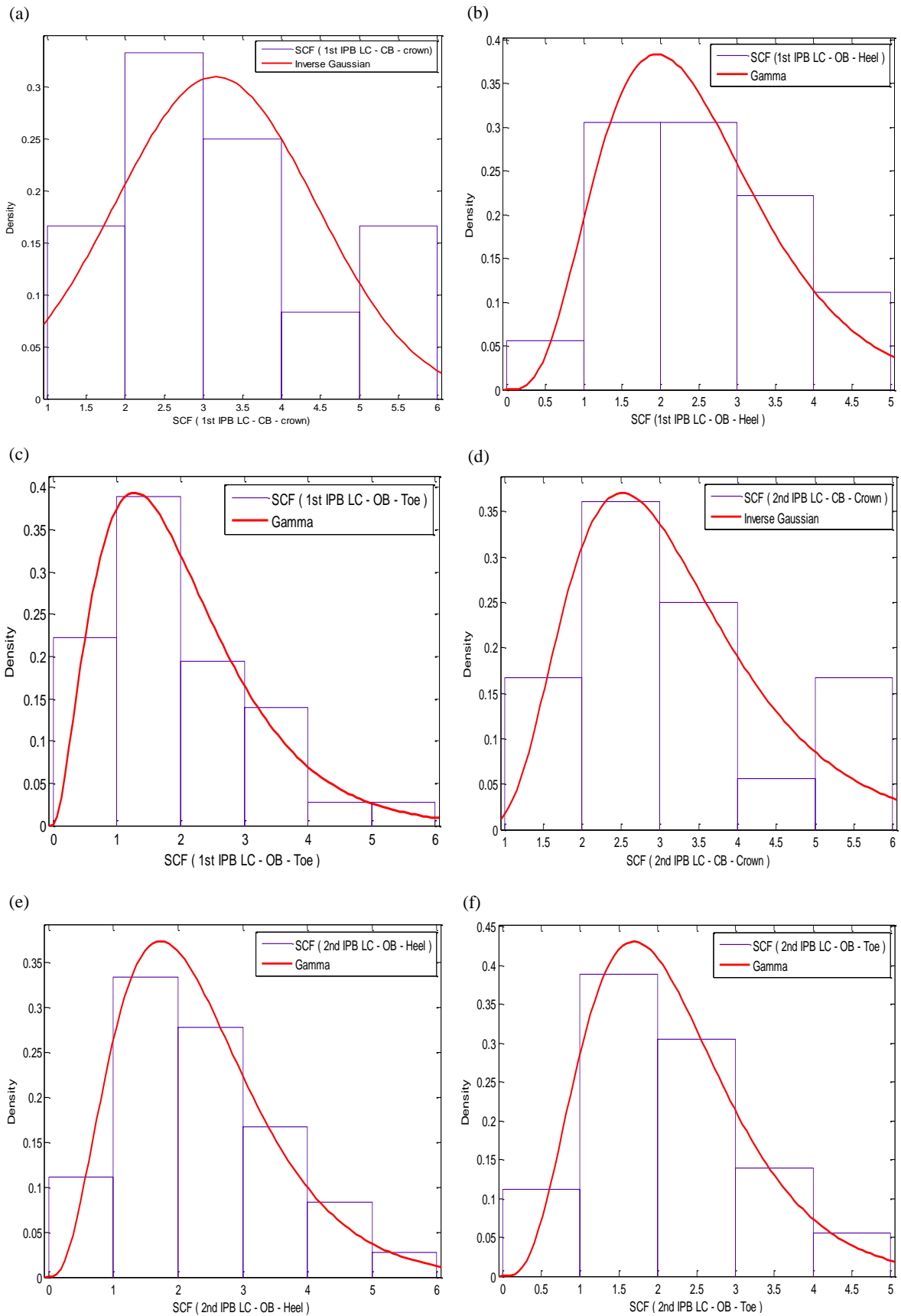
Figure 6. Proposed Inverse Gaussian and Gamma PDFs: (a) Sample 1 (1ˢᵗ *ILC*, *CB*, *C*), (b) Sample 2 (1ˢᵗ *ILC*, *OB*, *H*), (c) Sample 3 (1ˢᵗ *ILC*, *OB*, *T*), (d) Sample 4 (2ⁿᵈ *ILC*, *CB*, *C*), (e) Sample 5 (2ⁿᵈ *ILC*, *OB*, *H*), (f) Sample 6 (2ⁿᵈ *ILC*, *OB*, *T*), (g) Sample 7 (3ʳᵈ *ILC*, *OB*, *H*), (h) Sample 8 (3ʳᵈ *ILC*, *OB*, *T*), (i) Sample 9 (4ᵗʰ *ILC*, *OB*, *H*), (j) Sample 10 (4ᵗʰ *ILC*, *OB*, *T*); [KEY: *ILC*: IPB loading condition; *CB*: Central brace; *OB*: Outer brace; *C*: Crown; *H*: Heel; *T*: Toe]
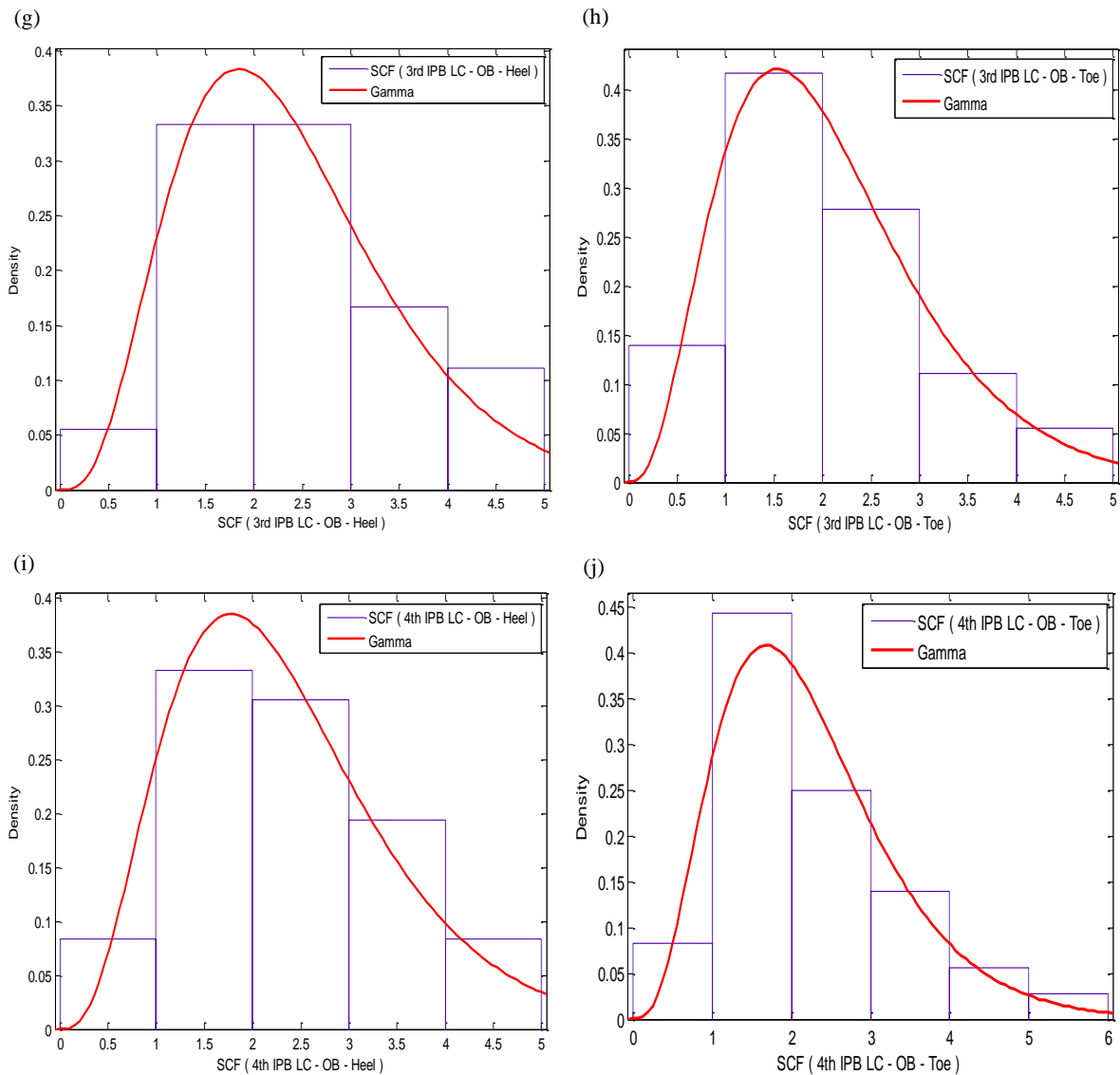
(g)

(h)

(i)

(j)

Fig. 6. *(Continued)*

8. Conclusions

In the present paper, results of 144 FE stress analyses, verified against experimental measurements, were used to develop a set of PDFs for the SCFs in uniplanar tubular KT-joints under four types of IPB moment load cases. Based on a parametric FE investigation, a sample database was created for the chord-side SCFs of central and outer braces; and density histograms were generated for respective samples. Nine theoretical PDFs were fitted to the developed histograms and the ML method was applied to evaluate the parameters of fitted PDFs. In each case, the Kolmogorov−Smirnov test was used to assess the goodness of fit. Finally, the Inverse Gaussian and Gamma models were proposed as the governing probability distribution functions for the central- and outer-brace SCFs, respectively. After substituting the values of estimated parameters, 10 fully defined PDFs were presented for the chord-side SCFs of central and outer braces in uniplanar tubular KT-joints under four types of IPB loading.

References

[1] American Petroleum Institute (API) (2007) Recommended practice for planning, designing and constructing fixed offshore platforms: Working stress design: RP2A-WSD. 21st Edition, Errata and Supplement 3, Washington DC, US.

[2] Yiyi C and Wei W (2003) Flexural behavior and resistance of uni-planar KK and X tubular joints. *Steel and Composite Structures* 3(2): 123−140.

[3] Choo YS (2005) Recent development and innovation in tubular structures. *Advances in Structural Engineering* 8(3): 217−230.

[4] Lie ST, Shao YB, Lee CK and Chiew SP (2006) Stress intensity factor solutions for semi-elliptical weld-toe cracks in tubular K-joints. *Advances in Structural Engineering* 9(1): 129−139.

[5] Gao F, Zhu HP and Liu XN (2013) Failure behavior of axially loaded tubular Y-joints under fire. *Advances in Structural Engineering* 16(9): 1523−1533.

[6] Liu H, Shao YB, Lu N and Wang Q (2015) Hysteresis of concrete-filled circular tubular

(CFCT) T-joints under axial load. *Steel and Composite Structures* 18(3): 739−756.

[7] Cui MJ and Shao YB (2015) Residual static strength of cracked concrete-filled circular steel tubular (CFCST) T-joint. *Steel and Composite Structures* 18(4): 1045−1062.

[8] Shao YB (2016) Static strength of collar-plate reinforced tubular T-joints under axial loading. *Steel and Composite Structures* 21(2): 323–342.

[9] Nassiraei H, Lotfollahi-Yaghin MA and Ahmadi H (2016) Structural behavior of tubular T/Y-joints with collar plate under static in-plane bending. *Journal of Constructional Steel Research* 123(8): 121−134.

[10] Efthymiou M and Durkin S (1985) Stress concentrations in T/Y and gap/overlap K-joints. *Proceedings of the Conference on Behavior of Offshore Structures*, Delft, Netherlands.

[11] Efthymiou M (1988) Development of SCF formulae and generalized influence functions for use in fatigue analysis. *OTJ 88*, Surrey, UK.

[12] Hellier AK, Connolly M and Dover WD (1990) Stress concentration factors for tubular Y and T-joints. *International Journal of Fatigue* 12: 13–23.

[13] Smedley P and Fisher P (1991) Stress concentration factors for simple tubular joints. *Proceedings of the International Offshore and Polar Engineering Conference (ISOPE)*, Edinburgh, UK.

[14] UK Health and Safety Executive (1997) OTH 354: stress concentration factors for simple tubular joints-assessment of existing and development of new parametric formulae. Prepared by Lloyd's Register of Shipping, London (UK): Health and Safety Executive.

[15] Karamanos SA, Romeijn A and Wardenier J (2000) Stress concentrations in tubular gap K-joints: mechanics and fatigue design. *Engineering Structures* 22: 4–14.

[16] Gho WM and Gao F (2004) Parametric equations for stress concentration factors in completely overlapped tubular K(N)-joints. *Journal of Constructional Steel Research* 60: 1761–1782.

[17] Gao F (2006) Stress and strain concentrations of completely overlapped tubular joints under lap brace OPB load. *Thin-Walled Structures* 44: 861−871.

[18] Gao F, Shao YB and Gho WM (2007) Stress and strain concentration factors of completely overlapped tubular joints under lap brace IPB load. *Journal of Constructional Steel Research* 63: 305–316.

[19] Morgan MR and Lee MMK (1998a) Parametric equations for distributions of stress concentration factors in tubular K-joints under out-of-plane moment loading. *International Journal of Fatigue* 20: 449–461.

[20] Morgan MR and Lee MMK (1998b) Prediction of stress concentrations and degrees of bending in axially loaded tubular K-joints. *Journal of Constructional Steel Research* 45(1): 67–97.

[21] Chang E and Dover WD (1999a) Parametric equations to predict stress distributions along the intersection of tubular X and DT-joints. *International Journal of Fatigue* 21: 619–635.

[22] Chang E and Dover WD (1999b) Prediction of stress distributions along the intersection of tubular Y and T-joints. *International Journal of Fatigue* 21: 361–381.

[23] Shao YB (2004) Proposed equations of stress concentration factor (SCF) for gap tubular K-joints subjected to bending load. *International Journal of Space Structures* 19: 137–147.

[24] Shao YB (2007) Geometrical effect on the stress distribution along weld toe for tubular T- and K-joints under axial loading. *Journal of Constructional Steel Research* 63: 1351–1360.

[25] Shao YB, Du ZF and Lie ST (2009) Prediction of hot spot stress distribution for tubular K-joints under basic loadings. *Journal of Constructional Steel Research* 65: 2011–2026.

[26] Lotfollahi-Yaghin MA and Ahmadi H (2010) Effect of geometrical parameters on SCF distribution along the weld toe of tubular KT-joints under balanced axial loads. *International Journal of Fatigue* 32: 703–719.

[27] Pang NL and Zhao XL (2009) Finite element analysis to determine stress concentration factors of dragline tubular joints. *Advances in Structural Engineering* 12(4): 463−478.

[28] Karamanos SA, Romeijn A, and Wardenier J (1990) Stress concentrations in multi-planar welded CHS XX-connections. *Journal of Constructional Steel Research* 50: 259–282.

[29] Chiew SP, Soh CK and Wu NW (2000) General SCF design equations for steel multiplanar tubular XX-joints. *International Journal of Fatigue* 22: 283–293.

[30] Wingerde AM, Packer JA and Wardenier J (2001) Simplified SCF formulae and graphs for CHS and RHS K- and KK-connections. *Journal of Constructional Steel Research* 57: 221–252.

[31] Karamanos SA, Romeijn A and Wardenier J (2002) SCF equations in multi-planar welded tubular DT-joints including bending effects. *Marine Structures* 15: 157–173.

[32] Ahmadi H, Lotfollahi-Yaghin MA and Aminfar MH (2012a) The development of fatigue design formulas for the outer brace SCFs in offshore three-planar tubular KT-joints. *Thin-Walled Structures* 58: 67–78.

[33] Ramachandra Murthy DS, Madhava Rao AG, Ghandi P and Pant PK (1992) Structural efficiency of internally ring stiffened steel tubular

joints. *Journal of Structural Engineering: ASCE* 118(11): 3016–3035.

[34] Nwosu DI, Swamidas ASJ and Munaswamy K (1995) Numerical stress analysis of internal ring-stiffened tubular T-joints. *Journal of Offshore Mechanics and Arctic Engineering* 117: 113–125.

[35] Ramachandra DS, Gandhi P, Raghava G and Madhava Rao AG (2000) Fatigue crack growth in stiffened steel tubular joints in seawater environment. *Engineering Structures* 22: 1390–1401.

[36] Hoon KH, Wong LK and Soh AK (2001) Experimental investigation of a doubler-plate reinforced tubular T-joint subjected to combined loadings. *Journal of Constructional Steel Research* 57: 1015–1039.

[37] Myers PT, Brennan FP and Dover WD (2001) The effect of rack/rib plate on the stress concentration factors in jack-up chords. *Marine Structures* 14: 485–505.

[38] Woghiren CO and Brennan FP (2009) Weld toe stress concentrations in multi planar stiffened tubular KK Joints. *International Journal of Fatigue* 31: 164–172.

[39] Ahmadi H, Lotfollahi-Yaghin MA, Shao YB and Aminfar MH (2012b) Parametric study and formulation of outer-brace geometric stress concentration factors in internally ring-stiffened tubular KT-joints of offshore structures. *Applied Ocean Research* 38: 74−91.

[40] Ahmadi H and Zavvar E (2015) Stress concentration factors induced by out-of-plane bending loads in ring-stiffened tubular KT-joints of jacket structures. *Thin-Walled Structures* 91: 82–95.

[41] Kirkemo F (1998) Applications of probabilistic fracture mechanics to offshore structures. *Applied Mechanics Review* 41: 61–84.

[42] Pillai TMM and Prasad AM (2000) Fatigue reliability analysis in time domain for inspection strategy of fixed offshore structures. *Ocean Engineering* 27: 167–186.

[43] Mosayyebi AR and Aghakuchak AA (2000) Fatigue reliability analysis of tubular joints of offshore structures using response surface method. *Asian Journal of Civil Engineering* 1: 75–87.

[44] Rajasankar J, Iyer NR and Appa Rao TVSR (2003) Structural integrity assessment of offshore tubular joints based on reliability analysis. *International Journal of Fatigue* 25: 609–619.

[45] Ahmadi H and Lotfollahi-Yaghin MA (2013) Effect of SCFs on S–N based fatigue reliability of multi-planar tubular DKT-joints of offshore jacket-type structures. Ships and Offshore Structures 8: 55−72.

[46] Ahmadi H, Lotfollahi-Yaghin MA and Aminfar MH (2011) Effect of stress concentration factors on the structural integrity assessment of multi-planar offshore tubular DKT-joints based on the fracture mechanics fatigue reliability approach. *Ocean Engineering* 38: 1883−1893.

[47] Ahmadi H, and Lotfollahi-Yaghin MA (2012) A probability distribution model for stress concentration factors in multi-planar tubular DKT-joints of steel offshore structures. *Applied Ocean Research* 34: 21−32.

[48] Ahmadi H, Mohammadi AH, and Yeganeh A (2015) Probability density functions of SCFs in internally ring-stiffened tubular KT-joints of offshore structures subjected to axial load. *Thin-Walled Structures* 94: 485–499.

[49] Ahmadi H, Mohammadi AH, Yeganeh A and Zavvar E (2016) Probabilistic analysis of stress concentration factors in tubular KT-joints reinforced with internal ring stiffeners under in-plane bending loads. *Thin-Walled Structures* 99: 58–75.

[50] Ahmadi H. (2016). A probability distribution model for SCFs in internally ring-stiffened tubular KT-joints of offshore structures subjected to out-of-plane bending loads. *Ocean Engineering* 116: 184–199.

[51] American Welding Society (AWS) (2002) Structural welding code: AWS D 1.1. Miami (FL), US.

[52] N'Diaye A, Hariri S, Pluvinage G and Azari Z (2007) Stress concentration factor analysis for notched welded tubular T-joints. *International Journal of Fatigue* 29: 1554–1570.

[53] IIW-XV-E (1999) Recommended fatigue design procedure for welded hollow section joints, IIW Docs, XV-1035-99/XIII-1804-99. Paris (France): International Institute of Welding.

[54] Ahmadi H and Lotfollahi-Yaghin MA (2013) Effect of SCFs on S–N based fatigue reliability of multi-planar tubular DKT-joints of offshore jacket-type structures. *Ships and Offshore Structures* 8: 55−72.

[55] Chang E, Dover WD (1996). Stress concentration factor parametric equations for tubular X and DT joints. *International Journal of Fatigue* 18(6): 363–387.

[56] Kottegoda NT and Rosso R (2008) Applied statistics for civil and environmental engineers. 2nd Edition, *Blackwell Publishing Ltd*, UK.